HHS Public Access

Author manuscript

J Neurosci Res. Author manuscript; available in PMC 2015 December 28.

Published in final edited form as:

J Neurosci Res. 2014 December ; 92(12): 1678–1689. doi:10.1002/jnr.23457.

Temporal Effects of Vascular Endothelial Growth Factor and cAMP on the Blood-Brain Barrier Solute permeability in vivo

Lingyan Shi, **Min Zeng**, and **Bingmei M. Fu***

Department of Biomedical Engineering, The City College of the City University of New York, 160 Convent Avenue, New York, NY 10031, USA

Abstract

To test the hypothesis that vascular endothelial growth factor (VEGF) can transiently increase the blood-brain barrier (BBB) permeability *P* as for peripheral microvessels, and elevation of 3,5-cyclic monophosphate (cAMP) levels can inhibit the VEGF-induced acute hyperpermeability, we employed multiphoton microscopy to quantify the cerebral microvessel permeability *P* to various-sized solutes under VEGF and cAMP treatments. The cerebral microcirculation was observed through a section of frontoparietal bone thinned with a micro-grinder. Fluorescein (MW 376Da), FITC-dextran-20k, -70k, or Alexa Fluor 488-IgG in 1% BSA mammalian Ringer's solution was injected into the cerebral circulation via the ipsilateral carotid artery by a syringe pump. Simultaneously, the temporal images were collected from the brain parenchyma ~100–200 μm below pia mater. *P* was determined from the rate of tissue solute accumulation around individual microvessels. Exposure to 1 nM VEGF transiently increased *P* to 2.2, 10.5, 9.8, and 12.8 times their control values, for fluorescein, dextran-20k, -70k, and IgG, respectively, within 30 s, and all returned to control in 2 min. After 20 min pretreatment of 2 mM cAMP analog, 8-bromo-cAMP, the initial increase by 1 nM VEGF was completely abolished in *P* to all solutes. The response pattern of *P* to VEGF and cAMP and the ratios of the peak to control values for rat cerebral microvessels are similar to those for rat mesenteric (peripheral) microvessels, except the ratios are higher in *P* of cerebral microvessels for the intermediate and large solutes. These results imply a new approach for delivering large therapeutic agents to brain.

Keywords

multi-photon microscopy; brain parenchyma; cerebral microvessel permeability to solutes; post-capillary venules; rat

Introduction

Due to its unique anatomical features, the blood-brain barrier (BBB) plays a protective role for the central nervous system (CNS) by restricting the entry of molecules into brain tissue from the circulating blood. Unfortunately, during cerebrovascular and neurological diseases, the BBB is comprised and its permeability can be increased by various types of stimuli

*Corresponding author Tel.: 212 650 7531; Fax: 212 650 6727, fu@ccny.cuny.edu.

The authors have not conflict of interests.

including cytokines, inflammatory mediators, metabolites of arachidonic acid, excitatory amino acids, nitric oxide and bacterial infection (Abbott 2000; Janigro et al. 1994; Kis et al. 2007; Mayhan 2001; Nakano et al. 1996; Sarker et al. 2000). Among cytokines, vascular endothelial growth factor (VEGF), which is upregulated in many brain diseases (Ohlin et al. 2011; Suidan et al. 2010), has been known to promote BBB leakage in the ischemic brain (Zhang et al. 2000), in brain tumors (Leung et al. 1997; Norden et al. 2008; Plate et al. 1992; Provias et al. 1997; Takano et al. 1996), and in CNS inflammatory diseases (Argaw et al. 2012) by disrupting endothelial tight junction proteins (Argaw et al. 2009). However, due to the limitation of measuring techniques and methods in previous studies, it is unclear how quickly and how much VEGF can increase the BBB permeability in vivo. For example, although magnetic resonance imaging (MRI) has advantages of non-invasive and high temporal resolution for the BBB permeability measurement (Armitage et al. 2011), even with contrast agents, its spatial resolution of ~100μm is not enough to detect the permeability change at the microvessel level. By using sub-micron resolution multiphoton fluorescence microscopy with a longer penetration depth into brain parenchyma, we first quantify temporal VEGF effects on the BBB permeability to various sized molecules.

Microvessel hyperpermeability is a critical step for the abnormal transport of molecules across the blood vessel wall and, thus, a critical step for many CNS disorders. In addition to anti-VEGF treatment for brain diseases (Batchelor et al. 2013; JuanYin et al. 2009; MacMillan et al. 2012; Miyatake et al. 2014; Soffietti et al. 2012; Ueta et al. 2011), other methods aiming at reinforcing microvessel wall integrity have been investigated to prevent the VEGF-induced BBB hyperpermeability. Previous studies have shown that elevated intracellular 3,5-cyclic monophosphate (cAMP) levels enhance endothelial junction barriers and thus reduce permeability in peripheral microvessels (Adamson et al. 1998; Fu et al. 1998; Fukuhara et al. 2005; Mehta and Malik 2006; Moore et al. 1998; Sayner 2011) and in cultured BBB models (Balyasnikova et al. 2000; Rubin et al. 1991; Wolburg et al. 1994). Studies on intact microvessels also showed that elevation of cAMP levels abolished the increase in the hydraulic conductivity stimulated by adenosine triphosphate (ATP) in frog and hamster mesenteric microvessels (He and Curry 1993) as well as in the solute permeability induced by VEGF in the same type of microvessels of frogs (Fu et al. 2006). Administration of a cAMP analogue abolished VEGF-induced dextran leakage in confluent BAEC (bovine aortic endothelial cell) monolayers (Murata et al. 2008).

Although elevation of cAMP levels has been found to significantly influence the permeability of peripheral microvessels and in vitro BBB, its role in regulating permeability of the BBB under physiological and pathological conditions is rarely known. Therefore, the second objective of this study is to quantify the cAMP effect on solute permeability of intact microvessels in rat brain parenchyma and the third objective is to test the hypothesis that elevation of cAMP levels can inhibit or attenuate the VEGF-induced hyperpermeability of the cerebral microvessels. Our results may suggest a potential approach for regulating BBB permeability for the treatment of various CNS diseases as well as improving brain drug delivery through systemic administration.

Materials and Methods

We measured P and its changes by VEGF or/and cAMP for the following solutes: IgG (MW 160 kDa), dextran-20k, -70k, and sodium fluorescein (MW 376Da). They have the representative sizes for the blood-borne molecules and also have similar sizes with the therapeutic antibodies, antibody fragments and agents for treating brain diseases including brain tumors (Evans et al. 2004), Alzheimer and Parkinson's disease (Friedman et al. 1997; Jansen 1994), and schizophrenia (Jones et al. 2006; Lieberman and Stroup 2011).

General preparation

All *in vivo* experiments were performed on adult female Sprague-Dawley rats (250–300 g, age 3–4 months) supplied by the Hilltop Lab Animals Inc. (Scottdale, PA). All procedures and animal use were approved by the Institutional Animal Care and Use Committee of the City College of New York. Rats were anesthetized with pentobarbital sodium given subcutaneously. The initial dose was 65 mg/kg and additional 3 mg/dose was given as needed. After a rat was anesthetized, the skull in the region of interest was exposed by shaving off the hair and cutting away the skin and connective tissue. A section (~ 4mm × 6mm) of the frontoparietal bone (left or right) was carefully ground with a high speed micro-grinder (0–50,000 rpm, DLT 50KBU; Brasseler USA, GA) until it became soft and translucent (Yuan et al. 2009). Artificial cerebrospinal fluid (ACSF) at room temperature was applied to the surface of the skull in order to remove the heat due to grinding. After grinding, the left or the right carotid artery was cannulated with tubing (PE50) which was connected to a syringe filled with needed solutions. The rat was then put on the stereotaxic instrument (David Kopf Instruments, Tujunga, CA) and its head was fixed firmly with two ear bars and a mouth clamp. A heating pad was put under the rat to maintain its body temperature during the experiment. The cerebral microvessels were observed by a multiphoton microscope through the thinned part of the skull. The control or test solution with and without fluorescently labeled solutes was then introduced into the cerebral circulation through the tubing by a syringe pump at a perfusion rate of 3 ml/min, the normal blood flow rate at the rat carotid artery. Usually it took ~10–15 s for the dye from the cannulation site at the carotid artery to the cerebral microvessels (Shi et al. 2014). Simultaneously, the images of cerebral microvessels and surrounding tissues in the region of interest were taken and used to determine the vessel permeability off-line. A single rat can only be used for one experimental condition and 1–3 vessels can be collected per rat for the permeability measurement. A total of 91 animals were used for this study.

Solutions and fluorescent test solutes preparation

Mammalian Ringer solution—Rat Ringer solution was used for all perfusates, which was composed of (in mM) NaCl 132, KCl 4.6, $MgSO_4$ 1.2, $CaCl_2$ 2.0, $NaHCO_3$ 5.0, glucose 5.5, and HEPES 20. The pH was balanced to 7.4–7.45 by adjusting the ratio of HEPES acid to base. Both the washout and fluorescent dye solutions additionally contained bovine serum albumin (BSA, A4378, Sigma, St. Louis, MO) at 10 mg/ml (Fu and Shen 2004; Yuan et al. 2009). Solutions were made fresh on the day of use to avoid binding to the serum albumin.

Artificial Cerebrospinal Fluid (ACSF)—The ACSF solution composition was (in mM) NaCl 110.5, KCl 4.7, $CaCl_2$ 2.5, KH_2PO_4 1.1, $MgSO_4 \cdot 7H_2O$ 1.25, $NaHCO_3$ 25 and HEPE 15 (Easton et al. 1997), and the solution was buffered to pH 7.4 ± 0.5.

Reagents—Vascular endothelial growth factor (VEGF) (human recombinant VEGF165, Peprotech, Rocky Hill, NJ) and 8-bromo-adenosine 3',5'-cyclic monophosphate (cAMP) (A9501, Sigma) were dissolved in the Ringer solution containing 10 mg/ml BSA (1% BSA Ringer).

Dye Solutions: Sodium Fluorescein, FITC-Dextrans, and IgG—Sodium fluorescein (F6377, Sigma, mol. wt. 376) was dissolved at the concentration of 0.125 mg/ml in 1% BSA Ringer.

FITC-dextran-20k (FD20s, Sigma, mol. wt. 20,000) and FITC-dextran-70k (FD70s, Sigma, mol. wt. 70,000) were used in the experiments at the concentration of 1 mg/ml in 1% BSA Ringer.

IgG (*Alexa Fluor® 488-ChromPure* mol. wt. 160,000) was also used in the experiments at the concentration of 0.5 mg/ml in 1% BSA Ringer.

To avoid hypoxia due to replacing the blood with the injected solutions since hypoxia can increase vessel permeability, all solutions were oxygenated by bubbling with the compressed gas composed of 95% oxygen and 5% carbon dioxide (Airgas, Bethlehem, PA) for 10 min before injection into the cerebral circulation.

Microscope preparation

Cerebral microvessels were observed under a 40× lens (NA0.8, water immersion, Olympus) by a 12-bit Ultima Multiphoton Microscopy System (Prairie Tech., Inc., WI) through the thinned section of rat brain. For FITC and Alexa Fluor® 488 with emission wavelength ~520 nm, the excitation wavelength was set to 800~850 nm to observe the cerebral microvessels ~100–200 μm below the pia mater. The solution with fluorescently labeled test solutes were introduced into the cerebral circulation via the ipsilateral carotid artery and the images of cerebral microvessels and surrounding tissues in the region of interest (ROI) were taken simultaneously. Images of ~239 μm × 239 μm ROI with 512 × 512 resolution were collected at a rate of ~ 1 frame/sec by our multiphoton system. The obtained images were then transferred to an image analysis workstation for determining vessel permeability off-line.

Determination of cerebral microvessel solute permeability P

We used the similar method as in our previous study for *P* of pial microvessels (Yuan et al. 2009) to determine *P* of cerebral microvessels ~100–200 μm below the pia mater. We chose post-capillary venules of 20–40 μm for the *P* measurement (Yuan et al. 2009). We followed the same method described in Easton et al (1997) to identify the post-capillary venules. In general, arterioles are long and straight with fewer branches than the venules, which are shorter and more tortuous. To further distinguish the arterioles and venules, before permeability measurement, we injected a small bolus of the fluorescent solution via the

carotid artery, the arterioles filled rapidly first and followed by a slower filling in venules (Easton et al. 1997). The *P* was determined off-line from the pre-collected images by using NIH Image-J. Figure 1a shows a typical image of a ROI (~239 μm × 239 μm) with several microvessels and surrounding brain tissue. The total fluorescence intensity I in a rectangular window including a vessel lumen and the surrounding tissue (Fig. 1a) was measured by Image-J. The measuring window was 50–100 μm long and 30–60 μm wide and was set at least 10 μm from the base of the bifurcation to avoid solute contamination from the side arms. The criteria for the size and placement of the measuring window were: 1) the vessel segment is straight; 2) the dye does not spread out of the window during the time for *P* measurement (10–60 s for the solutes in the current study); and 3) no dye contamination from the neighboring vessels into the window. When the criteria were satisfied, *P* was determined as $P = 1/\Delta I_0 * (dI/dt)_0 * r/2$ (Fu and Shen 2004; Yuan et al. 2009). Here ΔI_0 is the step increase of the fluorescence intensity in the window when the dye just fills up the vessel lumen (Fig. 1b). $(dI/dt)_0$ is the initial slope of the increasing curve of the total intensity I vs. time when the solute further transfers into the surrounding tissue, and *r* is the vessel radius. The increasing curve has a sharper slope for a smaller solute, indicating a higher permeability. From Figure 1b, *P* to NaF, Dex-70k, and IgG were calculated as 18.1, 1.22, and 0.50×10^{-7} cm/s, respectively, for vessels of diameter 36, 20 and 32 μm. During the time course of our measurement, the vessel diameter had negligible changes under the treatments.

The primary presumption in the calculation of *P* with the use of fluorescent solutes is that the fluorescence intensity I is a linear function of the number of solute molecules (concentration) in the measuring field. To test the linear range of the intensity vs. the concentration, we used the same instrument settings in the calibration experiments as those used in *in vivo* measurements. The details were described in (Yuan et al. 2009). We found that the relationship between the concentration and the fluorescence intensity was linear from 0.05 to 0.25 mg/ml for sodium fluorescein, from 0.2 to 2 mg/ml for FITC-dextran-20k and -70k, and from 0.1 to 1 mg/ml for IgG. We thus used 0.125 mg/ml, 1 mg/ml and 0.5 mg/ml, respectively, for sodium fluorescein, FITC-dextran-20k and 70k, and IgG in our permeability experiments.

Depth of light collection

During measurements of fluorescence intensity in the ROI, light collected from out-of-focus regions would contribute to the measured values. Therefore, *in vitro* experiments were performed to determine the depth of light collection. The procedures were described in the previous studies (Huxley et al. 1987; Yuan et al. 1993; Yuan et al. 2009). Briefly, six chambers with the depths of 10, 20, 40, 80, 170, and 340 μm were used to measure the fluorescence intensity of sodium fluorescein solution under the same experiments settings as those in *in vivo* permeability measurements. The chambers of 10–80 μm depth were constructed by sandwiching the membranes of 10 μm thickness from 24 transwell filters (Corning Inc., Corning, NY) in two coverslips. The 170 and 340 μm deep chambers were formed by placing one or two small 22 mm × 22 mm coverslips of thickness 170 μm in between two large 22 mm × 50 mm coverslips. The concentration-depth product was kept as a constant to make the fluorescein solution for the chambers of various depths (Yuan et al.

1993). The fluorescence intensity was measured for a window area of ~239 μm × 239 μm by focusing at the bottom surface of the chamber. The intensity was almost the same for the chamber with depth from 10 to 40 μm but decreased as the chamber depth increased from 40 to 340 μm (Fig. 2). Using a light collection index function (Yuan et al. 1993), we did the curve fitting for the measured intensity in the chambers of different depths (Fig. 2). The depth of light collection in our system is ~67 μm (z0 = 67.1 μm in the best-fitting index function), i.e., within this depth, fluorescence intensity is proportional to the number of fluorescent molecules and is independent of the chamber depth. Beyond this depth, our system can only collect partial or no light. This narrow depth of light collection in our system minimizes the light from other parts of the brain tissue, which allows us to more accurately determine the solute permeability of the cerebral microvessels in focus.

Experimental protocol

VEGF treatment—To investigate the effect of VEGF on the BBB permeability *P* to various solutes, for each solute, measurements were made by using a syringe pump to inject dye solution additionally containing 1 nM VEGF from the carotid artery. The concentration of VEGF was chosen to be consistent with that used in *P* measurement in rat mesenteric microvessels (Fu and Shen 2004). *P* was measured every 15–30 s in the first 2 min, and every 1 min for up to 5 min.

Similarly, the procedures of matched sham control groups were the same as those of test groups except using 1% BSA Ringer perfusates without VEGF.

cAMP treatment—To test the effect of cAMP on the BBB permeability *P* to various solutes, for each solute, baseline measurements were first made by injecting dye solution in 1%BSA Ringer. Then the syringe was replaced by two new syringes, one containing clear solution of 1% BSA Ringer with 4 mM cAMP, and another containing dye solution in 1% BSA Ringer with 2mM cAMP. First, the carotid artery was injected continuously with the clear solution of 4 mM cAMP for ~4 min at a speed of 1.5 ml/min and then switched to the dye solution containing 2mM cAMP for ~60 sec at 3 ml/min; images were taken during dye injection. This process was repeated every 5 min up to 20 min. The doubled concentration injected at half the speed for the clear solution provided a final concentration of 2 mM cAMP, which was consistent with previous studies (Fu et al. 2006; He and Curry 1993). The reduced injection speed prevents too much fluid from accumulating in the brain.

Similarly, the procedures of matched sham control groups were the same as those of test groups except using 1% BSA Ringer perfusates without cAMP.

cAMP pretreatment and VEGF/cAMP treatment on BBB permeability—To investigate solute permeability change affected by the combined effect of VEGF and cAMP, for each solute, baseline measurements were first made by injecting dye solution in 1%BSA Ringer. Then the syringe was replaced by two new syringes, one containing clear solution of 1% BSA Ringer with 4 mM cAMP, and another containing dye solution in 1% BSA Ringer with 2mM cAMP. *P* was measured every ~5 min up to 20 min as described above. After 20 min pretreatment of cAMP, the syringe was replaced by the one with the dye solution

containing 1 nM VEGF and 2 mM cAMP. *P* was measured every 15–30 s in the first 2 min, and every 1 min for up to 5 min.

The procedures for the matched sham control group were the same as the test group except that no cAMP was added into the pretreatment solution or dye solution.

Corrections for Influence of RBCs, free dye, and solvent drag on BBB permeability

The fluorescence dye solution was injected into the brain at the rate of 3 ml/min, the same as the normal blood perfusion rate (Brown et al. 2004; Garcia-Villalon et al. 1992). Although at this perfusion rate the blood was assumed to be replaced by the fluorescence solution, there was still residue blood (red blood cells, RBCs) in the cerebral microvessels, which would overestimate the measured BBB permeability by ~11%, as estimated in (Yuan et al. 2009).

In addition to RBCs, free dye would overestimate the permeability to fluorescently labeled solutes (Fu et al. 1998; Yuan et al. 2009). The influence of the free dye on the solute permeability was estimated by using equation $P^{correct} = [1/(1-F)]\ P^{measure} - [F/(1-F)]\ P^{freedye}$ (Fu et al. 1998), where $P^{measure}$ was measured permeability; $P^{freedye}$ was measured P^{NaFl} (18.9×10^{-7} cm/s) since the molecular weights of FITC (389.4) and Alexa Fluor 488 (643) are close to that of NaFl (376); F ~ 0.3% was the intensity ratio of the free dye filtrate to the original fluorescently labeled solution for FITC-dextrans and F ~ 0.1% for Alexa Fluor 488-IgG; $P^{correct}$ was the corrected solute permeability *P*.

The above apparent permeability *P* corrected for the RBCs and free dye still overestimates the true diffusive solute permeability P_d due to the coupling of solute flux with water flow (solvent drag). The P_d for FITC-dextrans and IgG were calculated by using the following equations (Fu et al. 1998; Fu and Shen 2003),

$$P = P_d \frac{P_e}{\exp(P_e - 1)} + L_p(1-\sigma)\Delta p_{eff} \quad (1)$$

$$P_e = \frac{L_p(1-\sigma)\Delta p_{eff}}{P_d} \quad (2)$$

where *P* is the measured apparent permeability, *Pe* is the Peclet number, *Lp* is the hydraulic conductivity of the microvessel, which is ~2.0×10^{-9} cm/s/cm H_2O for the cerebral microvessels (Kimura et al. 1993; Shi et al. 2014), σ is the reflection coefficient of the microvessel to the solute, and Δp_{eff} is the effective filtration pressure across the microvessel wall, obtained from

$$\Delta p_{eff} = \Delta p - \sigma^{albumin}\Delta\pi^{albumin} - \sigma^{dye-solute}\Delta\pi^{dye-solute} \quad (3)$$

where Δ*p* and Δπ are the hydrostatic and oncotic pressure differences across the microvessel wall. The superscript dye-solute can be FITC-dextrans or Alexa Fluor 488-IgG. σ of rat cerebral microvessels to the test solutes were estimated based on previous studies (Yuan et al. 2009) according to the molecule sizes. σ^{IgG}, $\sigma^{dextran\text{-}70k}$ (the same as $\sigma^{albumin}$) and $\sigma^{dextran\text{-}20k}$ were estimated to be 0.98, 0.94 and 0.5, respectively. Δ*p* in the cerebral

microvessel was ~10 cm H_2O, $\Delta\pi^{albumin}$ was 3.6 cm H_2O for 10 mg/ml BSA (Yuan et al. 2009).

Data analysis and statistics

P measured during the baseline period was averaged as the baseline *P*. This value was then used as a reference for all subsequent measurements on that vessel during the treatment. For the VEGF treatment, the control *P* measured during the sham control was used as the reference. Data were presented as means ± SE unless otherwise specified. ANOVA was applied to test statistical significance of the treatment over time and to between-group data for permeability differences at specific times. Significance was assumed for probability level $p < 0.05$.

Results

VEGF effects on BBB permeability

Figure 3 shows the temporal effects of 1 nM VEGF on BBB permeability *P* to fluorescein (Fig. 3a), Dex-20k (Fig. 3b), Dex-70k(Fig. 3c) and IgG(Fig. 3d), respectively. For each solute, *P* measured in each vessel (■) was normalized by the mean value measured in the sham control experiment (○). For all the solutes, *P* was increased transiently by 1nM VEGF in as short as 15sec, peaked at ~30 sec and returned to the baseline in ~2 min. The mean *P* measured at the peak of the response was 41.0 ± 2.6 × 10^{-7} cm/s (n = 9, range: 29.8 – 53.1 × 10^{-7} cm/s) for sodium fluorescein (NaF), a 2.2 ± 0.14–fold increase compared with the control P^{NaFl} of 18.9 ± 0.52 × 10^{-7} cm/s. Correspondingly, the mean peak $P^{Dex\text{-}20k}$ was 24.7 ± 3.0 × 10^{-7} cm/s (n = 8, range: 12.6 – 37.0 × 10^{-7} cm/s), a 10.5 ± 1.3–fold increase compared with the control $P^{Dex\text{-}20k}$ of 2.34 ± 0.22 × 10^{-7} cm/s; the mean peak $P^{Dex\text{-}70k}$ was 13.4 ± 2.3 × 10^{-7} cm/s (n = 9, range: 4.3 – 26.4 × 10^{-7} cm/s), a 9.8 ± 1.7–fold increase compared with the control $P^{Dex\text{-}70k}$ of 1.37 ± 0.11 × 10^{-7} cm/s; the mean peak P^{IgG} was 8.1 ± 0.5 × 10^{-7} cm/s (n = 9, range: 6.4 – 10.8 × 10^{-7} cm/s), a 12.8 ± 0.8–fold increase compared with the control P^{IgG} of 0.63 ± 0.04 × 10^{-7} cm/s. Table 1 summarizes the control and VEGF-induced peak values of apparent permeability *P* for all the solutes.

Table 2 also summarizes the corrected *P* for the RBCs, free dye and solvent drag, under control and that at the peak under VEGF treatment. Under the peak increase by VEGF, in the correction for the solvent drag (see Eqs. 1, 2), *Lp* was estimated at 10-fold that of the control, similar to that used in (Fu and Shen 2003; Fu and Shen 2004).

cAMP effects on BBB permeability

Figure 4 demonstrates the temporal effects of 2mM 8-bromo-cAMP on BBB permeability to fluorescein (Fig. 4a), Dex-20k (Fig. 4b), Dex-70k(Fig. 4c) and IgG(Fig. 4d), respectively. For each solute, *P* measured in every vessel (■) was normalized by its baseline value and compared with the sham control (○) at the same time. For all the solutes, *P* decreased after 5 min 2 mM cAMP treatment, but not significantly until after 15 min treatment ($p < 0.05$). After ~20 min treatment, P^{NaFl} decreased from 19.1± 1.48 × 10^{-7} cm/s to 12.3 ± 1.2 × 10^{-7} cm/s; $P^{Dex\text{-}20k}$ decreased from 1.76 ± 0.13 × 10^{-7} cm/s to 0.95 ± 0.13 × 10^{-7} cm/s; $P^{Dex\text{-}7\text{-}0k}$ decreased from 1.47 ± 0.25× 10^{-7} cm/s to 0.70 ± 0.09 × 10^{-7} cm/s; P^{IgG} decreased from

$0.54 \pm 0.10 \times 10^{-7}$ cm/s to $0.31 \pm 0.05 \times 10^{-7}$ cm/s. Table 3 summarizes these data and the ratio of the decreased *P* after 20 min cAMP treatment to the baseline for all the solutes. Table 4 also summarizes the corrected *P* for the RBCs, free dye and solvent drag, under control and after 20 min treatment of 2 mM cAMP. In the correction for the solvent drag, *Lp* was estimated at half of the control after 20 min cAMP treatment, similar to that used in (Fu et al. 2006).

Combined effects of cAMP and VEGF on BBB permeability

In addition to regulating BBB permeability by VEGF and cAMP alone, we also investigated the combined effects of cAMP and VEGF as in the previous study for mesenteric microvessel permeability (Fu et al. 2006). Figure 5 shows the P^{IgG} as a function of time during 20 min pretreatment of 2mM cAMP and for another 5 min treatment under 2mM cAMP and 1nM VEGF(■, BSA-cAMP-cAMP/VEGF). As a comparison, Fig. 5 also demonstrates the control group by 1 nM VEGF only (o, BSA-BSA-VEGF). In the control group, after 20 min sham experiment, 1 nM VEGF transiently increased P^{IgG} in as soon as ~15 sec. P^{IgG} peaked at ~30 sec, reaching a 11.27 ± 2.74-fold increase compared to the baseline, and returned to the baseline in ~2 min, the same pattern as shown in Fig. 3d. In contrast, after 20 min pretreatment of 2 mM 8-bromo-cAMP, the transient increase in P^{IgG} by 1 nM VEGF was completely abolished, at ~30 sec, P^{IgG} was $0.35 \pm 0.11 \times 10^{-7}$ cm/s, 0.87 ± 0.23 times baseline ($p > 0.1$). Pretreatment of 2 mM 8-bromo-cAMP for 20 min can also abolish the transient increase by VEGF in *P* to fluorescein, Dex-20k, and Dex-70k (data not shown here).

Figure 6 summarizes the combined effects of cAMP and VEGF on *P* to all the solutes. Pretreatment of 2 mM cAMP for 20 min reduced P^{NaFl} to 0.63 ± 0.08 (n=11, $p < 0.03$), $P^{Dex\text{-}20k}$ to 0.54 ± 0.07 (n=8, $p < 0.05$), $P^{Dex\text{-}7\text{-}0k}$ to 0.49 ± 0.09 (n=8, $p < 0.04$), and P^{IgG} to 0.43 ± 0.06 (n=7, $p < 0.04$), of their baseline values, respectively, and completely abolished the transient increase in *P* by 1nM VEGF ($p > 0.1$). In contrast, after pretreatment of 1%BSA Ringer for 20 min, *P* to none of the solutes had significantly changes ($p > 0.3$), but 1nM VEGF transiently increased P^{NaFl} to 1.99 ± 0.2 (n=7, $p < 0.01$), $P^{Dex\text{-}20k}$ to 10.3 ± 1.1 (n=5, $p < 0.03$), $P^{Dex\text{-}7\text{-}0k}$ to 9.0 ± 0.91 (n=5, $p < 0.04$), and P^{IgG} to 10.5 ± 2.3 (n=6, $p < 0.04$), of their baseline values, respectively, at the peak after ~30 sec treatment.

Discussion

By employing high resolution multiphoton microscopy, we were able to determine the temporal effects of VEGF and cAMP on the BBB permeability for individual microvessels in the rat brain parenchyma. Compared to previous methods, our method is direct and more sensitive. It enables us to distinguish the BBB permeability to various-sized solutes (Fig. 1b) and detect the transient change in the BBB permeability to the same sized solute, and to avoid the contamination from the out of focus fluorescent light due to a narrow depth of light collection (Fig. 2) by using a high numerical aperture lens. The BBB permeability measured in the current study is local, more quantitative and reliable.

Regulation of BBB permeability by VEGF

In consistent with previous studies that VEGF promotes BBB leakages (Argaw et al. 2009; Zhang et al. 2000), using *in vivo* quantitative multiphoton microscopy with a deeper penetration length into brain parenchyma, we further examined the temporal effect of VEGF on solute permeability (*P*) of individual cerebral microvessels ~100–200 μm below the pia mater. Exposure to 1 nM VEGF transiently increased cerebral microvessel *P* to 2.2, 10.5, 9.8, and 12.8 times their control values, for fluorescein, dextran-20k, -70k, and IgG, respectively, within 30 s, and all returned to control in 2 min. These temporal patterns of VEGF effects on *P* of the BBB are similar to those on *P* of peripheral (mesenteric) microvessels (Fu and Shen 2003; Fu and Shen 2004) except the ratios are higher in *P* of cerebral microvessels for the intermediate and large sized solutes.

On the luminal surface of both peripheral and BBB endothelium, there is a surface glycocalyx layer consisting of various proteoglycan and glycosaminoglycans (Fu and Tarbell 2013; Li et al. 2010). Different from the peripheral microvessel wall which is only formed by endothelium, in the BBB, pericytes attach to the abluminal membrane of the endothelium at irregular intervals. Both endothelial cells and pericytes are surrounded by a uniform and narrow matrix-like basement membrane (BM) which contains collagen type IV, heparan sulfate proteoglycans, and various extracellular matrix proteins (Leblond and Inoue 1989; Miosge 2001). On the tissue side, the BM is ensheathed by astrocyte foot processes which cover ~98% of the brain microvasculature surface (Cohen et al. 1995; Pardridge 1999). The BBB endothelium also has much less fenestration and more intensive tight junctions (Hawkins and Davis 2005). The differential anatomic features of the BBB may explain the higher increase in *P* of BBB to larger solutes by VEGF, the reason of which is that VEGF can regulate other structural components of the BBB in addition to endothelium. As predicted in (Fu and Shen 2003), VEGF acutely increases peripheral microvessel *P* by increasing the gap between adjacent endothelial cells and partial degradation of the endothelial surface glycocalyx. To account for higher increase in *P* of the BBB to larger solutes, VEGF may also increase the width of the BM as well as degrade the extracellular matrix in the BM as extracellular matrix provides a large resistance to large solute transport (Li et al. 2010). Longer term VEGF treatment can increase the BBB leakage by disrupting the tight junctions (Argaw et al. 2009), however, the short term (minutes) effect may just transiently increase the gap spacing between adjacent endothelial cells. Further investigation is needed to test these predictions.

Table 2 summarizes the control and VEGF-induced peak values for *P* of the BBB to all-sized solutes after correction for RBC, free dye, and the solvent drag effect. Due to much smaller hydraulic conductivity of the BBB compared to that of a peripheral microvessel wall (about two orders of magnitude) (Kimura et al. 1993; Yuan et al. 2009), the solvent drag contributes much less to the apparent permeability of cerebral microvessels than to that of peripheral (mesenteric) microvessels (Fu and Shen 2003; Fu and Shen 2004) under both control and VEGF conditions, even we assumed that VEGF can increase hydraulic conductivity of the BBB by 10-fold. This finding implies that although we can use VEGF to transiently increase *P* of BBB to large molecules (molecular weight larger than 20k) by ~10-fold, we cannot further increase the trans-BBB transport of large molecules by enhancing

the transmural pressure difference (solvent drag). Another finding is that VEGF only moderately enhances the trans-BBB transport of small molecules (molecular weight ~ several hundred). This may be beneficial when delivering large molecular weight drugs to brain through systemic administration without significantly losing needed nutrients, salts and other small molecules in the blood.

Regulation of BBB permeability by cAMP

Previous in vivo and in vitro studies have shown that elevation of intracellular cAMP can enhance the endothelial barrier functions (Mehta and Malik 2006; Rubin et al. 1991; Sayner 2011) by increasing the number of tight junction strands (Adamson et al. 1998), the complexity of the tight junctions (Wolburg et al. 1994) and the expression of the intercellular adhesion molecules (Balyasnikova et al. 2000) in between adjacent endothelial cells. In spite of additional structural components of the BBB, our results demonstrated the same effect of cAMP on its barrier function. In ~15 min after cAMP treatment, *P* of the BBB to all-sized solutes decreases significantly from its baseline. Compared to *P* of the peripheral (mesenteric) microvessel, which has a significant decrease in ~5 min (Fu et al. 1998; Fu et al. 2006), the ~10 min delay may be due to the delay from the cAMP injection from the carotid artery and the mixing with the residue blood in the microvessel, or due to the additional structures of the BBB. The slightly less decreasing levels (the ratios to control are higher, Table 3) than those in *P* of the mesenteric microvessel (Fu et al. 2006) may also due to the same reason. These results suggest that the surrounding structures for the endothelium of the BBB serve as a stabilizer to keep transport across the BBB relatively constant regardless the fluctuations in the circulating blood or brain tissue.

Further stabilizing function of cAMP has been shown to abolish the permeability increase by inflammatory mediators, cytokines and toxins in various experimental models. Simultaneous stimulation of adenylate cyclase and phosphodiesterase inhibition was highly effective in inhibiting permeability increases induced by H_2O_2 in an isolated rabbit lung (Seeger et al. 1995) and other stimuli in the lung (Sayner 2011). Elevation of cAMP also blocks monolayer permeability stimulated by histamine (Sheldon et al. 1993), phorbol myristate acetate (Garcia et al. 1995), thrombin, hemolysin (Suttorp et al. 1993), and pertussis toxin (Bruckener et al. 2003). Previous studies on intact peripheral microvessels also confirms the blocking effect of a cAMP analog on inflammatory stimulation (He and Curry 1993) and VEGF (Fu et al. 2006). Solutions containing 1 nM VEGF stimulate a two- to seven-fold increase in *P* of mesenteric microvessels to various-sized solutes. This transient increase was nearly abolished by 20 min pretreatment with 8-bromo-cAMP (2 mM). In consistent with the cAMP effect on VEGF-induced hyperpermeability of peripheral microvessels, our results have shown that 20 min pretreatment of 2 mM cAMP analog completely diminish the transient increase by VEGF in *P* of the BBB. cAMP behaves as a permeability defender against VEGF for the BBB as well. The possible mechanism for cAMP to abolish the BBB permeability increase by VEGF may be similar to that in the peripheral microvessel. The pretreatment of cAMP can increase the number of tight junction strands in the paracellular pathway of the microvessel wall (Adamson et al. 1998) and can diminish the transient increase by VEGF, as predicted by Fu et al. (Fu et al. 2006).

In the current study, we only measured the permeability of post-capillary venules with diameter of 20–40 μm for the following reasons: 1) To avoid the influence of smooth muscle cells at arteries, arterioles and large venules, which would contract under stimuli and affect the permeability measurement; 2) For unclear reasons, certain hyper-permeability was reported to primarily occur in post-capillary venules or venules (Egawa et al. 2013; Mayhan 2001); 3) Previous studies found that VEGF and cAMP can modulate permeability of mesenteric (peripheral) post-capillary venules (Fu and Shen 2003; Fu and Shen 2004; Fu et al. 2006); 4) Our previous studies on the BBB permeability were also conducted on this type of post-capillary venules (Shi et al. 2014; Yuan et al. 2009). In the current study, since we used high spatial resolution and narrow depth of light collection imaging settings to more accurately determine the permeability of the individual cerebral microvessel, we only focused on the region of interest containing most of post-capillary venules. In the future, we can use the same technique to quantify the BBB permeability of other types of vessels.

In summary, by using a minimally-invasive multiphoton microscopy, we have quantified *P* of the BBB in rat brain parenchyma and its regulation by VEGF and cAMP. Compared to previous studies which only measured the BBB leakage, this is the first study that determines the true BBB solute permeability and its temporal changes by VEGF and cAMP in live animals. The results not only provide insights to new treatment methods for many cerebrovascular and neurological diseases, but also suggest a new approach for delivering large molecular weight therapeutic agents (e.g. antibodies and their fragments) to brain through systemic administration.

Acknowledgement

We thank Mr. Dawi Shin for his help in determining the depth of light collection.

Supported partially by National Science Foundation CBET 0754158, NIH-CA153325 and CUNY SEED grant 93348-14-01 1

References

Abbott NJ. Inflammatory mediators and modulation of blood-brain barrier permeability. Cell Mol Neurobiol. 2000; 20(2):131–147. [PubMed: 10696506]

Adamson RH, Liu B, Fry GN, Rubin LL, Curry FE. Microvascular permeability and number of tight junctions are modulated by cAMP. Am J Physiol. 1998; 274(6 Pt 2):H1885–H1894. [PubMed: 9841516]

Argaw AT, Asp L, Zhang J, Navrazhina K, Pham T, Mariani JN, Mahase S, Dutta DJ, Seto J, Kramer EG, Ferrara N, Sofroniew MV, John GR. Astrocyte-derived VEGF-A drives blood-brain barrier disruption in CNS inflammatory disease. J Clin Invest. 2012; 122(7):2454–2468. [PubMed: 22653056]

Argaw AT, Gurfein BT, Zhang Y, Zameer A, John GR. VEGF-mediated disruption of endothelial CLN-5 promotes blood-brain barrier breakdown. Proc Natl Acad Sci U S A. 2009; 106(6):1977–1982. [PubMed: 19174516]

Armitage PA, Farrall AJ, Carpenter TK, Doubal FN, Wardlaw JM. Use of dynamic contrast-enhanced MRI to measure subtle blood-brain barrier abnormalities. Magn Reson Imaging. 2011; 29(3):305–314. [PubMed: 21030178]

Balyasnikova IV, Pelligrino DA, Greenwood J, Adamson P, Dragon S, Raza H, Galea E. Cyclic adenosine monophosphate regulates the expression of the intercellular adhesion molecule and the inducible nitric oxide synthase in brain endothelial cells. J Cereb Blood Flow Metab. 2000; 20(4):688–699. [PubMed: 10779013]

Batchelor TT, Gerstner ER, Emblem KE, Duda DG, Kalpathy-Cramer J, Snuderl M, Ancukiewicz M, Polaskova P, Pinho MC, Jennings D, Plotkin SR, Chi AS, Eichler AF, Dietrich J, Hochberg FH, Lu-Emerson C, Iafrate AJ, Ivy SP, Rosen BR, Loeffler JS, Wen PY, Sorensen AG, Jain RK. Improved tumor oxygenation and survival in glioblastoma patients who show increased blood perfusion after cediranib and chemoradiation. P Natl Acad Sci USA. 2013; 110(47):19059–19064.

Brown RC, Egleton RD, Davis TP. Mannitol opening of the blood-brain barrier: regional variation in the permeability of sucrose, but not 86Rb+ or albumin. Brain Res. 2004; 1014(1–2):221–227. [PubMed: 15213006]

Bruckener KE, el Baya A, Galla HJ, Schmidt MA. Permeabilization in a cerebral endothelial barrier model by pertussis toxin involves the PKC effector pathway and is abolished by elevated levels of cAMP. Journal of Cell Science. 2003; 116(9):1837–1846. [PubMed: 12665564]

Cohen Z, Ehret M, Maitre M, Hamel E. Ultrastructural Analysis of Tryptophan-Hydroxylase Immunoreactive Nerve-Terminals in the Rat Cerebral-Cortex and Hippocampus - Their Associations with Local Blood-Vessels. Neuroscience. 1995; 66(3):555–569. [PubMed: 7644020]

Easton AS, Sarker MH, Fraser PA. Two components of blood-brain barrier disruption in the rat. The Journal of physiology. 1997; 503(Pt 3):613–623. [PubMed: 9379415]

Egawa G, Nakamizo S, Natsuaki Y, Doi H, Miyachi Y, Kabashima K. Intravital analysis of vascular permeability in mice using two-photon microscopy. Sci Rep-Uk. 2013; 3

Evans AJ, James JJ, Cornford EJ, Chan SY, Burrell HC, Pinder SE, Gutteridge E, Robertson JF, Hornbuckle J, Cheung KL. Brain metastases from breast cancer: identification of a high-risk group. Clin Oncol (R Coll Radiol). 2004; 16(5):345–349. [PubMed: 15341438]

Friedman JH, Koller WC, Lannon MC, Busenbark K, Swanson-Hyland E, Smith D. Benztropine versus clozapine for the treatment of tremor in Parkinson's disease. Neurology. 1997; 48(4):1077–1081. [PubMed: 9109903]

Fu BM, Adamson RH, Curry FE. Test of a two-pathway model for small-solute exchange across the capillary wall. The American journal of physiology. 1998; 274(6 Pt 2):H2062–H2073. [PubMed: 9841533]

Fu BM, Shen S. Structural mechanisms of acute VEGF effect on microvessel permeability. American journal of physiology. 2003; 284(6):H2124–H2135. [PubMed: 12560209]

Fu BM, Shen S. Acute VEGF effect on solute permeability of mammalian microvessels in vivo. Microvasc Res. 2004; 68(1):51–62. [PubMed: 15219420]

Fu BM, Shen S, Chen B. Structural mechanisms in the abolishment of VEGF-induced microvascular hyperpermeability by cAMP. J Biomech Eng. 2006; 128(3):317–328. [PubMed: 16706581]

Fu BM, Tarbell JM. Mechano-sensing and transduction by endothelial surface glycocalyx: composition, structure, and function. Wiley Interdiscip Rev Syst Biol Med. 2013; 5(3):381–390. [PubMed: 23401243]

Fukuhara S, Sakurai A, Sano H, Yamagishi A, Somekawa S, Takakura N, Saito Y, Kangawa K, Mochizuki N. Cyclic AMP potentiates vascular endothelial cadherin-mediated cell-cell contact to enhance endothelial barrier function through an Epac-Rap1 signaling pathway. Mol Cell Biol. 2005; 25(1):136–146. [PubMed: 15601837]

Garcia-Villalon AL, Roda JM, Alvarez F, Gomez B, Dieguez G. Carotid blood flow in anesthetized rats: effects of carotid ligation and anastomosis. Microsurgery. 1992; 13(5):258–261. [PubMed: 1406230]

Garcia JG, Davis HW, Patterson CE. Regulation of endothelial cell gap formation and barrier dysfunction: role of myosin light chain phosphorylation. J Cell Physiol. 1995; 163(3):510–522. [PubMed: 7775594]

Hawkins BT, Davis TP. The blood-brain barrier/neurovascular unit in health and disease. Pharmacol Rev. 2005; 57(2):173–185. [PubMed: 15914466]

He P, Curry FE. Differential actions of cAMP on endothelial [Ca2+]i and permeability in microvessels exposed to ATP. Am J Physiol. 1993; 265(3 Pt 2):H1019–H1023. [PubMed: 8214108]

Huxley VH, Curry FE, Adamson RH. Quantitative fluorescence microscopy on single capillaries: alpha-lactalbumin transport. The American journal of physiology. 1987; 252(1 Pt 2):H188–H197. [PubMed: 3492924]

Janigro D, West GA, Nguyen TS, Winn HR. Regulation of blood-brain barrier endothelial cells by nitric oxide. Circ Res. 1994; 75(3):528–538. [PubMed: 8062426]

Jansen EN. Clozapine in the treatment of tremor in Parkinson's disease. Acta Neurol Scand. 1994; 89(4):262–265. [PubMed: 8042443]

Jones PB, Barnes TR, Davies L, Dunn G, Lloyd H, Hayhurst KP, Murray RM, Markwick A, Lewis SW. Randomized controlled trial of the effect on Quality of Life of second- vs first-generation antipsychotic drugs in schizophrenia: Cost Utility of the Latest Antipsychotic Drugs in Schizophrenia Study (CUtLASS 1). Arch Gen Psychiatry. 2006; 63(10):1079–1087. [PubMed: 17015810]

Juan Yin J, Tracy K, Zhang L, Munasinghe J, Shapiro E, Koretsky A, Kelly K. Noninvasive imaging of the functional effects of anti-VEGF therapy on tumor cell extravasation and regional blood volume in an experimental brain metastasis model. Clin Exp Metastasis. 2009; 26(5):403–414. [PubMed: 19277878]

Kimura M, Dietrich HH, Huxley VH, Reichner DR, Dacey RG Jr. Measurement of hydraulic conductivity in isolated arterioles of rat brain cortex. The American journal of physiology. 1993; 264(6 Pt 2):H1788–H1797. [PubMed: 8322907]

Kis, B.; Ueta, Y.; Busiji, DW. Peptide mediators of the brain endothelium. In: Lajtha, A.; Reith, MEA., editors. Handbook of neurochemistry and molecular neurobiology. 3rd ed. New York: Springer; 2007. p. 191-208.

Leblond CP, Inoue S. Structure, composition, and assembly of basement membrane. The American journal of anatomy. 1989; 185(4):367–390. [PubMed: 2675590]

Leung SY, Chan AS, Wong MP, Yuen ST, Cheung N, Chung LP. Expression of vascular endothelial growth factor and its receptors in pilocytic astrocytoma. Am J Surg Pathol. 1997; 21(8):941–950. [PubMed: 9255258]

Li G, Yuan W, Fu BM. A model for the blood-brain barrier permeability to water and small solutes. J Biomech. 2010; 43(11):2133–2140. [PubMed: 20434157]

Lieberman JA, Stroup TS. The NIMH-CATIE Schizophrenia Study: what did we learn? Am J Psychiatry. 2011; 168(8):770–775. [PubMed: 21813492]

MacMillan CJ, Furlong SJ, Doucette CD, Chen PL, Hoskin DW, Easton AS. Bevacizumab Diminishes Experimental Autoimmune Encephalomyelitis by Inhibiting Spinal Cord Angiogenesis and Reducing Peripheral T-Cell Responses. J Neuropath Exp Neur. 2012; 71(11):983–999. [PubMed: 23037326]

Mayhan WG. Regulation of blood-brain barrier permeability. Microcirculation. 2001; 8(2):89–104. [PubMed: 11379794]

Mehta D, Malik AB. Signaling mechanisms regulating endothelial permeability. Physiol Rev. 2006; 86(1):279–367. [PubMed: 16371600]

Miosge N. The ultrastructural composition of basement membranes in vivo. Histology and histopathology. 2001; 16(4):1239–1248. [PubMed: 11642743]

Miyatake SI, Kawabata S, Hiramatsu R, Furuse M, Kuroiwa T, Suzuki M. Boron neutron capture therapy with bevacizumab may prolong the survival of recurrent malignant glioma patients: four cases. Radiat Oncol. 2014; 9

Moore TM, Chetham PM, Kelly JJ, Stevens T. Signal transduction and regulation of lung endothelial cell permeability. Interaction between calcium and cAMP. Am J Physiol. 1998; 275(2 Pt 1):L203–L222. [PubMed: 9700080]

Murata T, Lin MI, Aritake K, Matsumoto S, Narumiya S, Ozaki H, Urade Y, Hori M, Sessa WC. Role of prostaglandin D2 receptor DP as a suppressor of tumor hyperpermeability and angiogenesis in vivo. Proc Natl Acad Sci U S A. 2008; 105(50):20009–20014. [PubMed: 19060214]

Nakano S, Matsukado K, Black KL. Increased brain tumor microvessel permeability after intracarotid bradykinin infusion is mediated by nitric oxide. Cancer Res. 1996; 56(17):4027–4031. [PubMed: 8752174]

Norden AD, Drappatz J, Wen PY. Novel anti-angiogenic therapies for malignant gliomas. Lancet Neurol. 2008; 7(12):1152–1160. [PubMed: 19007739]

Ohlin KE, Francardo V, Lindgren HS, Sillivan SE, O'Sullivan SS, Luksik AS, Vassoler FM, Lees AJ, Konradi C, Cenci MA. Vascular endothelial growth factor is upregulated by L-dopa in the

parkinsonian brain: implications for the development of dyskinesia. Brain. 2011; 134(Pt 8):2339–2357. [PubMed: 21771855]

Pardridge WM. Blood-brain barrier biology and methodology. Journal of Neurovirology. 1999; 5(6): 556–569. [PubMed: 10602397]

Plate KH, Breier G, Weich HA, Risau W. Vascular Endothelial Growth-Factor Is a Potential Tumor Angiogenesis Factor in Human Gliomas Invivo. Nature. 1992; 359(6398):845–848. [PubMed: 1279432]

Provias J, Claffey K, delAguila L, Lau N, Feldkamp M, Guha A. Meningiomas: role of vascular endothelial growth factor/vascular permeability factor in angiogenesis and peritumoral edema. Neurosurgery. 1997; 40(5):1016–1026. [PubMed: 9149260]

Rubin LL, Hall DE, Porter S, Barbu K, Cannon C, Horner HC, Janatpour M, Liaw CW, Manning K, Morales J, Tanner LI, Tomaselli KJ, Bard F. A Cell-Culture Model of the Blood-Brain-Barrier. J Cell Biol. 1991; 115(6):1725–1735. [PubMed: 1661734]

Sarker MH, Hu DE, Fraser PA. Acute effects of bradykinin on cerebral microvascular permeability in the anaesthetized rat. J Physiol. 2000; 528(Pt 1):177–187. [PubMed: 11018116]

Sayner SL. Emerging themes of cAMP regulation of the pulmonary endothelial barrier. Am J Physiol Lung Cell Mol Physiol. 2011; 300(5):L667–L678. [PubMed: 21335524]

Seeger W, Hansen T, Rossig R, Schmehl T, Schutte H, Kramer HJ, Walmrath D, Weissmann N, Grimminger F, Suttorp N. Hydrogen Peroxide-Induced Increase in Lung Endothelial and Epithelial Permeability - Effect of Adenylate-Cyclase Stimulation and Phosphodiesterase Inhibition. Microvasc Res. 1995; 50(1):1–17. [PubMed: 7476570]

Sheldon A, Booth FW, Kirby CR. cAMP levels in fast- and slow-twitch skeletal muscle after an acute bout of aerobic exercise. Am J Physiol. 1993; 264(6 Pt 1):C1500–C1504. [PubMed: 8392799]

Shi L, Zeng M, Sun Y, Fu BM. Quantification of blood-brain barrier solute permeability and brain transport by multiphoton microscopy. J Biomech Eng. 2014; 136(3):031005. [PubMed: 24193698]

Soffietti R, Trevisan E, Ruda R. Targeted therapy in brain metastasis. Curr Opin Oncol. 2012; 24(6): 679–686. [PubMed: 22820413]

Suidan GL, Dickerson JW, Chen Y, McDole JR, Tripathi P, Pirko I, Seroogy KB, Johnson AJ. CD8 T cell-initiated vascular endothelial growth factor expression promotes centralnervous system vascular permeability under neuroinflammatory conditions. J Immunol. 2010; 184(2):1031–1040. [PubMed: 20008293]

Suttorp N, Weber U, Welsch T, Schudt C. Role of phosphodiesterases in the regulation of endothelial permeability in vitro. J Clin Invest. 1993; 91(4):1421–1428. [PubMed: 8386187]

Takano S, Yoshii Y, Kondo S, Suzuki H, Maruno T, Shirai S, Nose T. Concentration of vascular endothelial growth factor in the serum and tumor tissue of brain tumor patients. Cancer Research. 1996; 56(9):2185–2190. [PubMed: 8616870]

Ueta T, Mori H, Kunimatsu A, Yamaguchi T, Tamaki Y, Yanagi Y. Stroke and Anti-VEGF Therapy. Ophthalmology. 2011; 118(10):2093-U2247. [PubMed: 21968167]

Wolburg H, Neuhaus J, Kniesel U, Krauss B, Schmid EM, Ocalan M, Farrell C, Risau W. Modulation of tight junction structure in blood-brain barrier endothelial cells. Effects of tissue culture, second messengers and cocultured astrocytes. J Cell Sci. 1994; 107(Pt 5):1347–1357. [PubMed: 7929640]

Yuan F, Leunig M, Berk DA, Jain RK. Microvascular permeability of albumin, vascular surface area, and vascular volume measured in human adenocarcinoma LS174T using dorsal chamber in SCID mice. Microvasc Res. 1993; 45(3):269–289. [PubMed: 8321142]

Yuan W, Lv Y, Zeng M, Fu BM. Non-invasive measurement of solute permeability in cerebral microvessels of the rat. Microvasc Res. 2009; 77(2):166–173. [PubMed: 18838082]

Zhang ZG, Zhang L, Jiang Q, Zhang R, Davies K, Powers C, Bruggen N, Chopp M. VEGF enhances angiogenesis and promotes blood-brain barrier leakage in the ischemic brain. J Clin Invest. 2000; 106(7):829–838. [PubMed: 11018070]

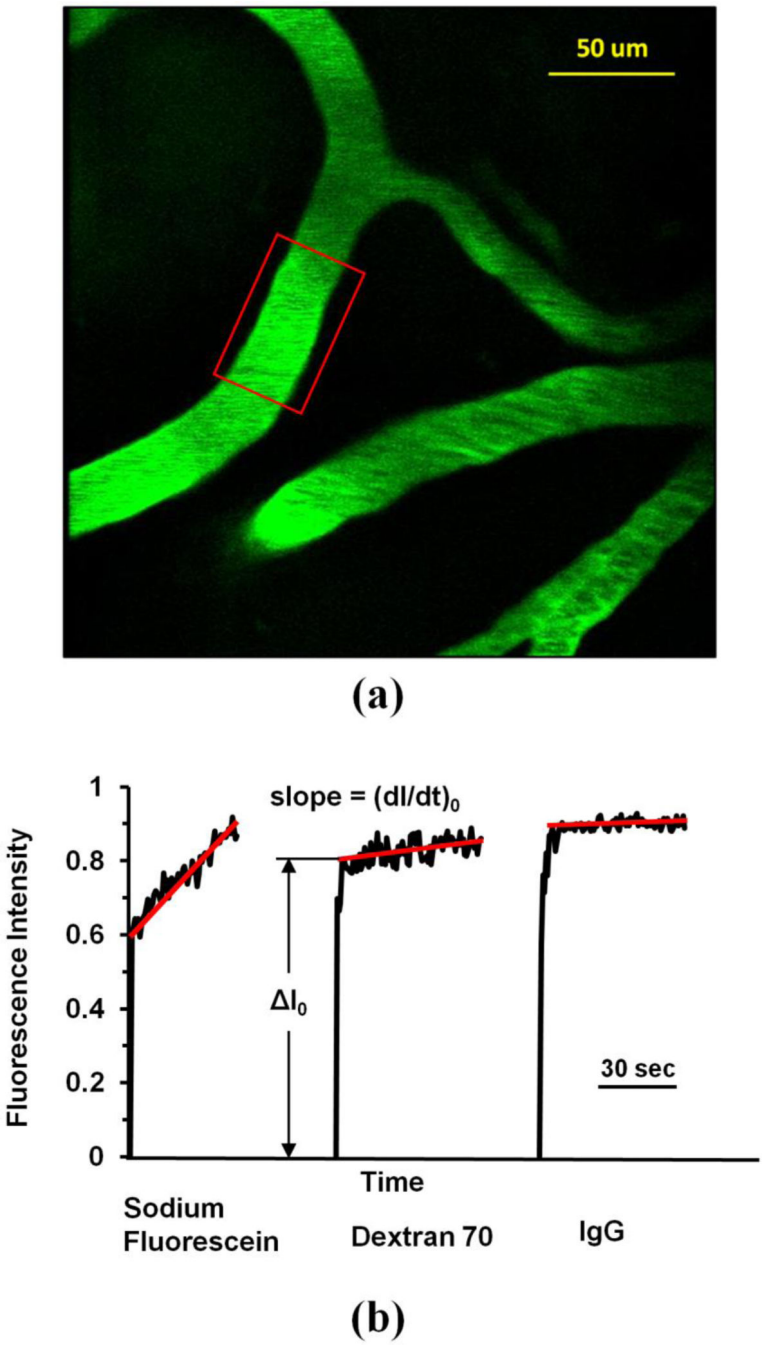

Figure 1.

(**a**) Illustration of the scanning region comprising of several microvessels ~100–200μm below the pia mater. The region area is ~239 μm × 239 μm. The red frame enclosed area is the region of interest (ROI) used to determine the BBB permeability *P* to a solute. (**b**) Total fluorescence intensity in the ROI as a function of perfusion time. Fluorescence intensity in the figure is proportional to the total mass of solute accumulated in the measuring region surrounding the microvessel. The slope of regression line over the initial linear accumulation $(dI/dt)_0$ is used to determine permeability $P = 1/\Delta I_0 * (dI/dt)_0 * r/2$. ΔI_0 is the step intensity

increase when the dye just fills up the vessel lumen, and *r* is the radius of the vessel. Typical intensity vs. time curves are shown for the determination of *P* to the small (sodium fluorescein), medium-large (Dex-70K) and large (IgG) sized solutes.

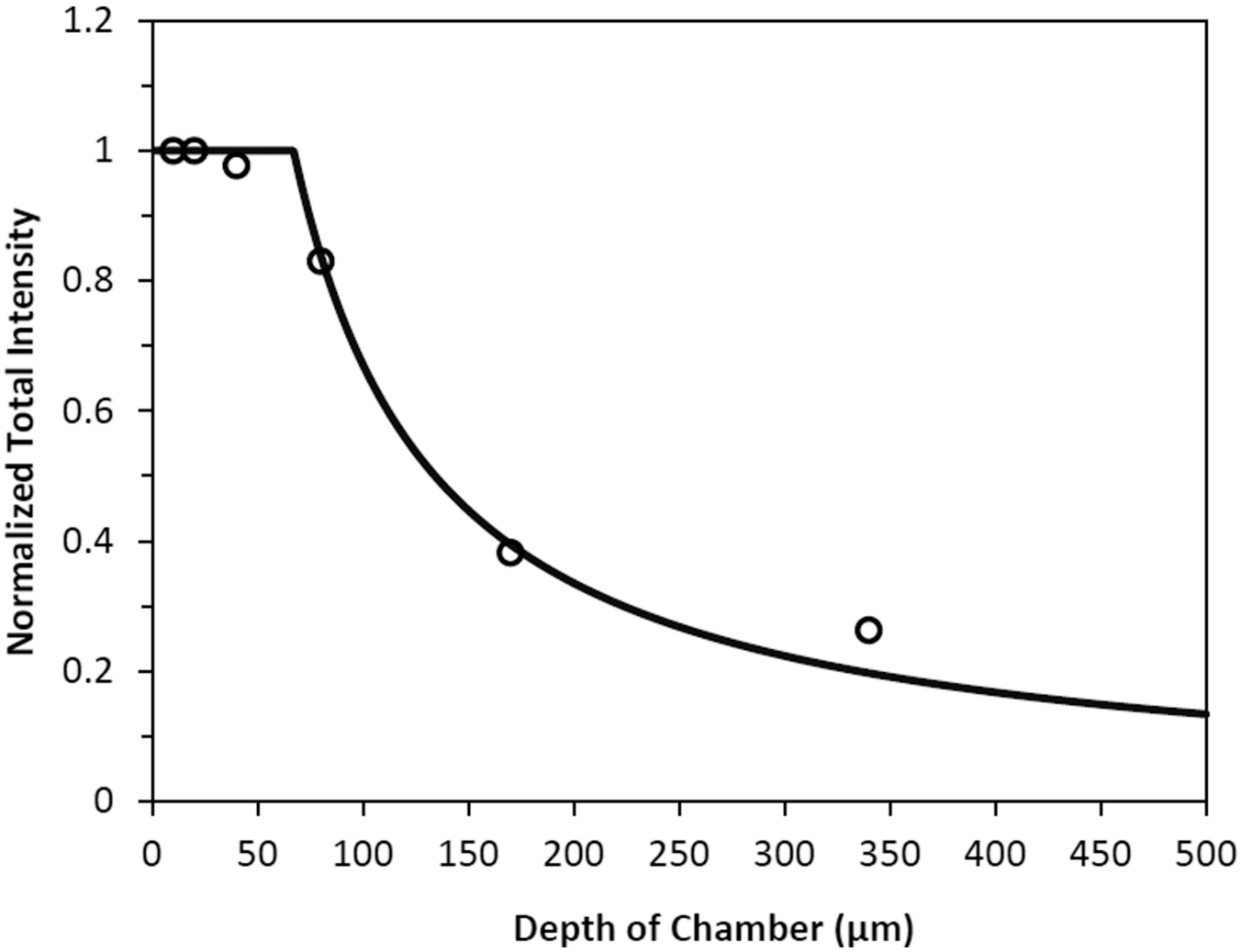

Figure 2.

Depth of light collection of our imaging system. Samples of NaFl solutions were prepared such that concentration-depth product was maintained constant. The total fluorescence intensity, which was normalized by that measured using the 10 μm-depth chamber, was plotted for the chambers with the depth 10, 20, 40, 80, 170, and 340 μm (○). The solid line is the curve fitting for the measured intensity values using a light collection index function in (Yuan et al. 1993).

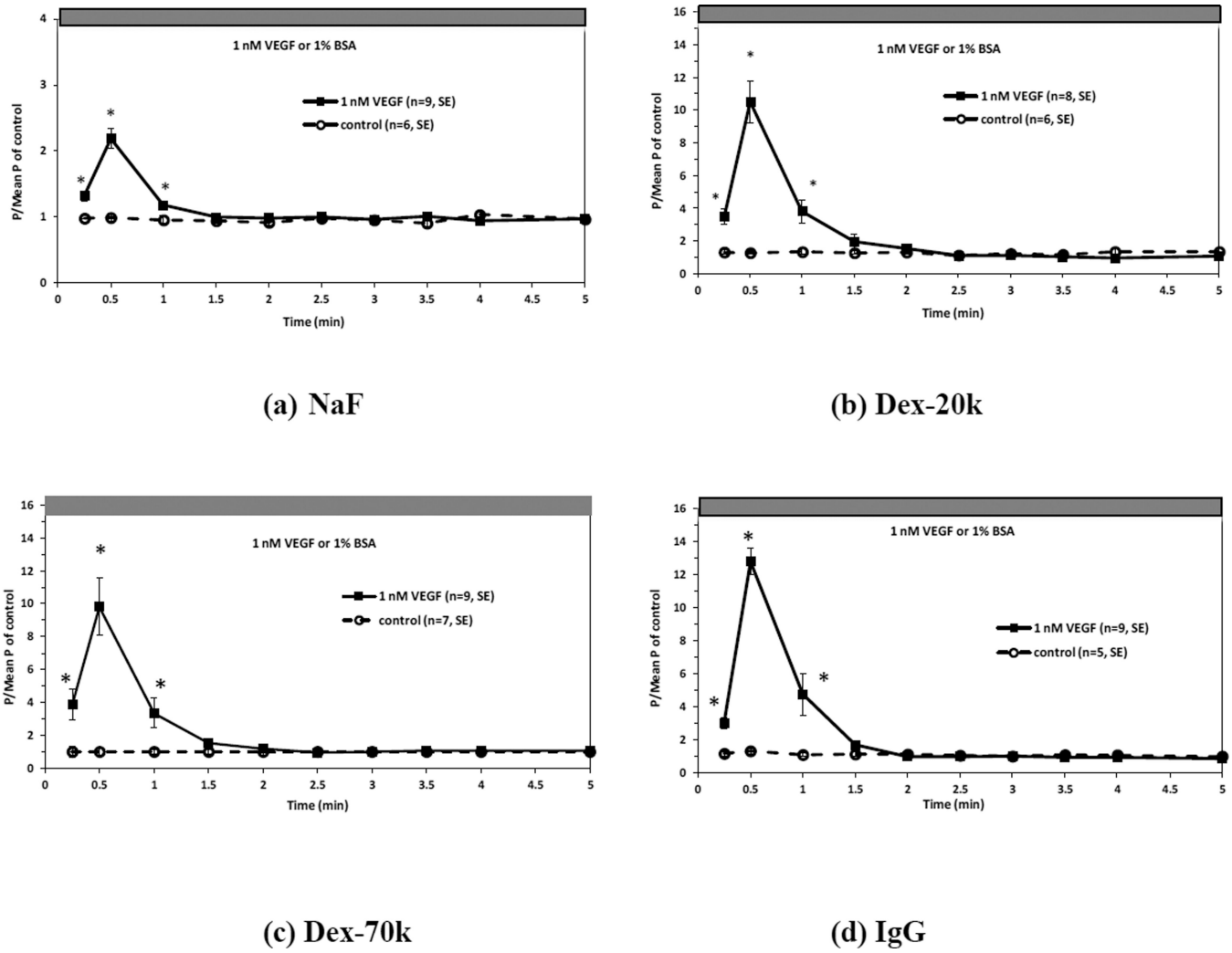

Figure 3.

Effect of 1 nM VEGF on the BBB permeability *P* to (**a**) sodium fluorescein, (**b**) Dex-20k, (**c**) Dex-70k, and (**d**) IgG. Mean ± SE *P* relative to the mean control value was plotted as a function of time. The solid line with ■ is for the test group and the dashed line with ○ is for the control group. * $p < 0.05$ compared with the control.

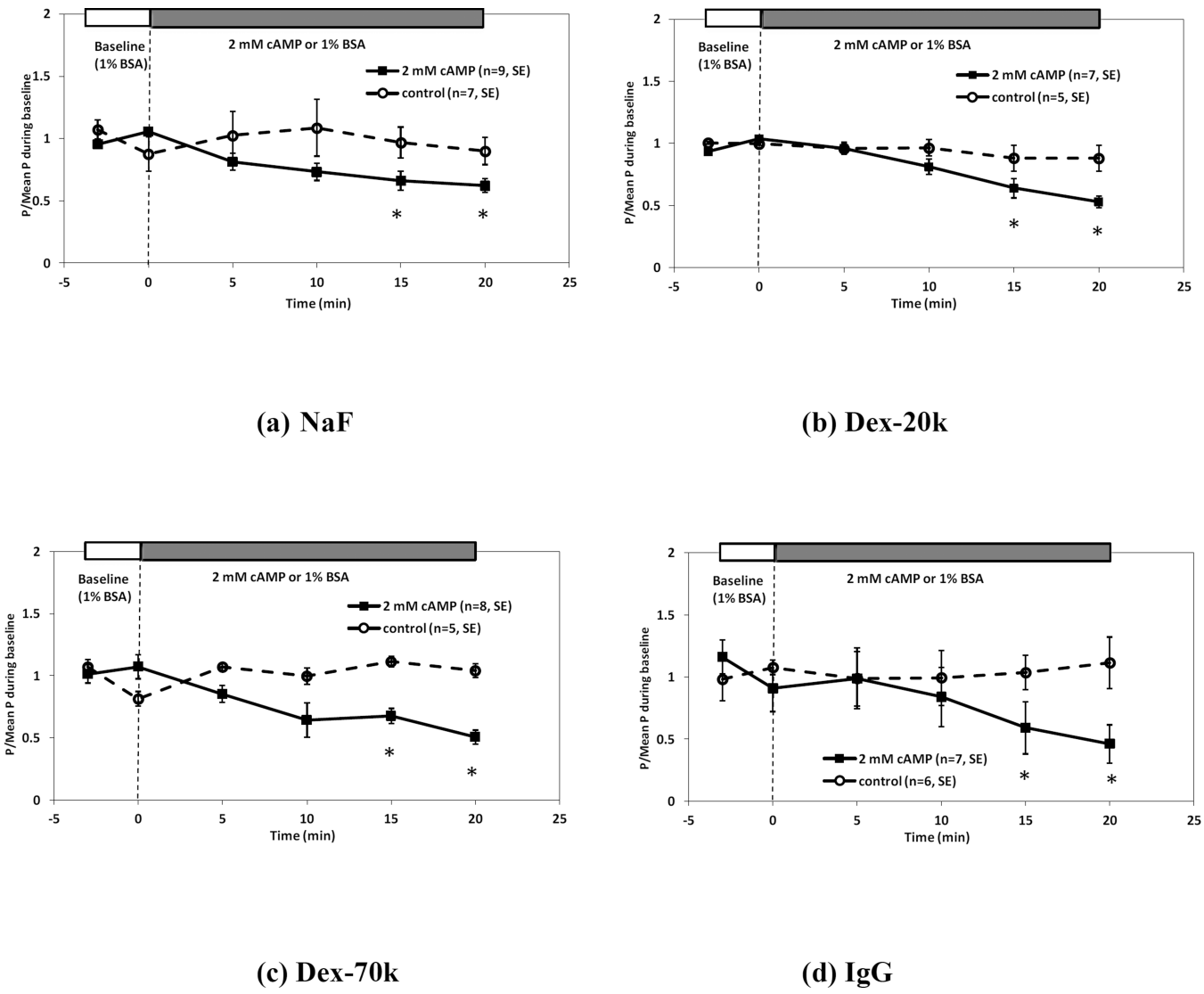

Figure 4.

Effect of 2 mM cAMP on the BBB permeability *P* to (**a**) sodium fluorescein, (**b**) Dex-20k, (**c**) Dex-70k, and (**d**) IgG. Mean ± SE *P* relative to baseline value was plotted as a function of time. The solid line with ■ is for the test group and the dashed line with ○ is for the control group. * $p < 0.05$ compared with the baseline.

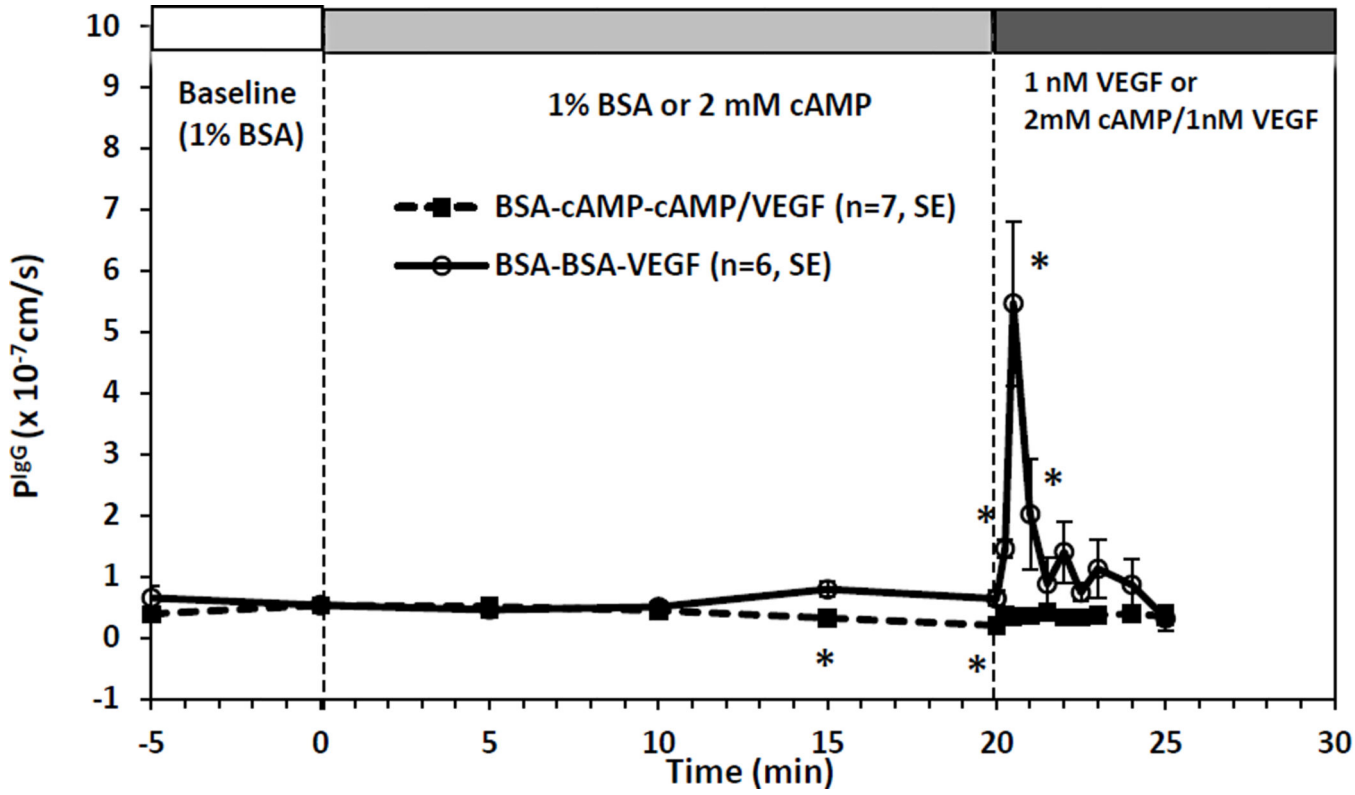

Figure 5.

Effect of 20 min pretreatment with 2 mM cAMP on 1 nM VEGF-induced vessel hyperpermeability to IgG in rat cerebral microvessels. *P* (mean ± SE) was plotted as a function of time. The solid line with the ■ is for the test group and the dashed line with ○ is for the control group. * $p < 0.05$ compared with the baseline.

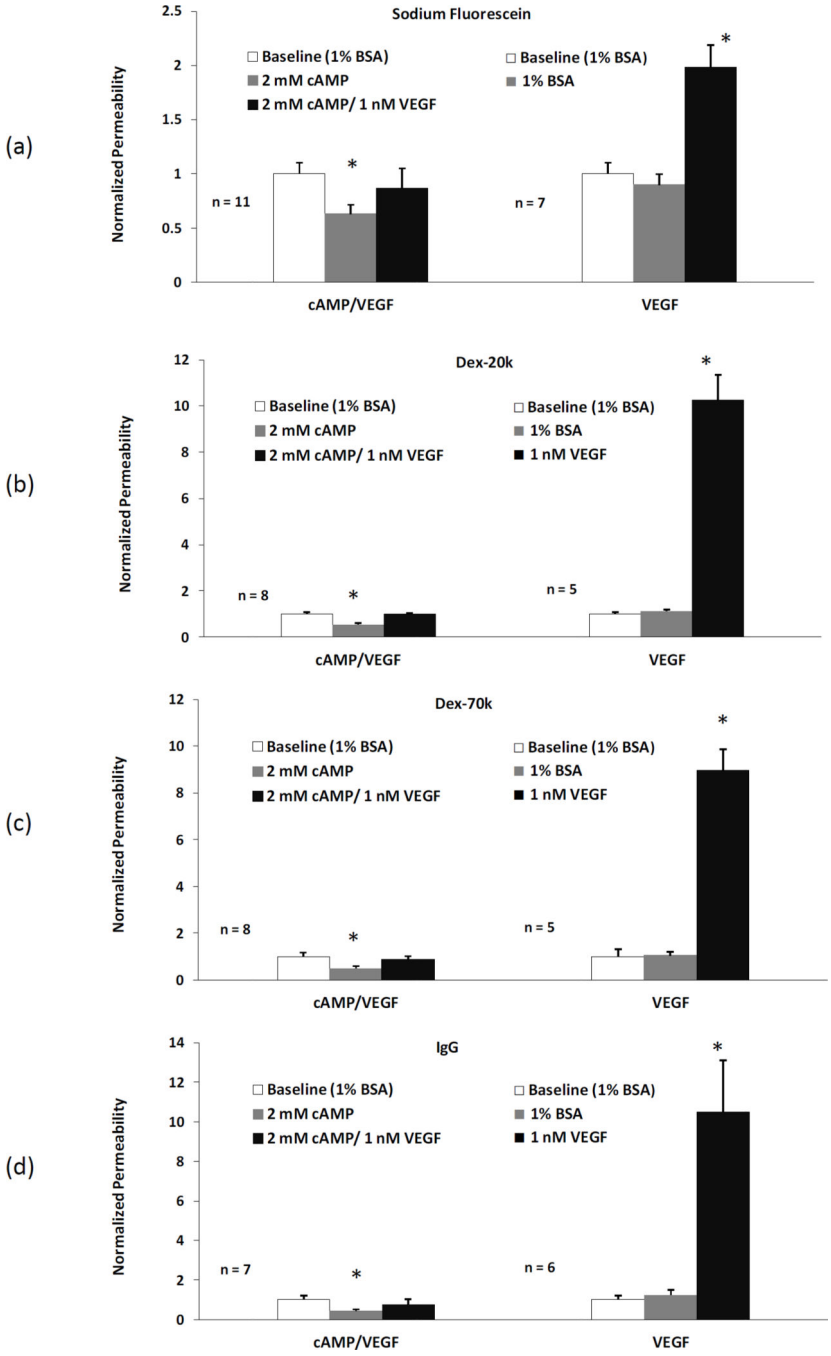

Figure 6.

Comparison of apparent *P* (mean ± SE) in the test group (20 min pretreatment with cAMP and then VEGF/cAMP), left panel, and that in the control group (no cAMP) , right panel, for (**a**) sodium fluorescein, (**b**) Dex-20k, (**c**) Dex-70k, and (**d**) IgG. The first bar in each group is the baseline with 1%BSA Ringer perfusion, the second bar in the test group is *P* after 20 min cAMP treatment and the third bar is *P* after ~30 sec VEGF/cAMP treatment. For comparison, the second bar in the control group is *P* after 20 min 1%BSA Ringer and the

third bar is *P* after ~30 sec VEGF treatment. *$p < 0.05$ compared with the baseline in each group.

Table 1

Control P and peak P under 1 nM VEGF treatment

Solute	Control (× 10^{-7} cm/s)	Peak (× 10^{-7} cm/s)	Ratio	*p-value*
NaFl	18.9 ± 0.52 (n=6)	41.0 ± 2.6 (n=9)	2.2 ± 0.14	< 0.0001
Dex-20k	2.34 ± 0.22 (n=6)	24.7 ± 3.0 (n=8)	10.5 ± 1.3	< 0.0001
Dex-70k	1.37 ± 0.11 (n=7)	13.4 ± 2.3 (n=9)	9.8 ± 1.7	< 0.0001
IgG	0.63 ± 0.04 (n=5)	8.1 ± 0.5 (n=9)	12.8 ± 0.8	< 0.0001

Values are mean ± SE; n, number of vessels.

Table 2

Corrected control *P* and peak *P* under 1 nM VEGF treatment

Solute	*P*(measured) ($\times 10^{-7}$ cm/s)	*P*(corrected for RBC) ($\times 10^{-7}$ cm/s)	*P*(corrected for RBC and free dye) ($\times 10^{-7}$ cm/s)	*Pd* (corrected for RBC, free dye, and solvent drag) ($\times 10^{-7}$ cm/s)
Control (Lp = 2 × 10^{-9} cm/s/cm H_2O)				
NaFl (n=6)	18.9 ± 0.52	16.78 ± 0.46	16.78 ± 0.46	16.78 ± 0.46
Dex 20k (n=6)	2.34 ± 0.22	2.08 ± 0.19	2.03 ± 0.19	2.00 ± 0.19
Dex 70k (n=7)	1.37 ± 0.11	1.22 ± 0.10	1.20 ± 0.10	1.19 ± 0.10
IgG (n=5)	0.63 ± 0.04	0.56 ± 0.03	0.55 ± 0.03	0.54 ± 0.03
VEGF (Lp = 2 × 10^{-8} cm/s/cm H_2O)				
NaFl (n=9)	41.0 ± 2.58	36.5 ± 2.30	36.5 ± 2.31	36.4 ± 2.31
Dex 20k (n=8)	24.7 ± 3.02	22.0 ± 2.69	21.9 ± 2.70	21.3 ± 2.70
Dex 70k (n=9)	13.4 ± 2.27	11.9 ± 2.02	11.8 ± 2.03	11.0 ± 2.03
IgG (n=9)	8.1 ± 0.47	7.2 ± 0.42	7.2 ± 0.42	6.7 ± 0.42

Values are mean ± SE; n, number of vessels.

Table 3

Baseline *P* and that after 20 min treatment of 2 mM cAMP

Solute	n	Baseline (× 10^{-7} cm/s)	cAMP (× 10^{-7} cm/s)	Ratio	*p-value*
NaFl	9	19.1 ± 1.48	12.3 ± 1.2	0.62 ± 0.06	0.002
Dex-20k	7	1.76 ± 0.13	0.95 ± 0.13	0.53 ± 0.05	< 0.0001
Dex-70k	8	1.47 ± 0.25	0.70 ± 0.09	0.51 ± 0.07	0.013
IgG	7	0.54 ± 0.10	0.31 ± 0.04	0.46 ± 0.15	0.05

Values are mean ± SE; n, number of vessels.

Table 4

Corrected *P* for the baseline and that after 20 min treatment of 2 mM cAMP

Solute	*P*(measured) ($\times 10^{-7}$ cm/s)	*P*(corrected for RBC) ($\times 10^{-7}$ cm/s)	*P*(corrected for RBC and free dye) ($\times 10^{-7}$ cm/s)	P_d (corrected for RBC, free dye, and solvent drag) ($\times 10^{-7}$ cm/s)
Baseline (Lp = 2 × 10^{-9} cm/s/cm H_2O)				
NaFl (n=9)	19.1 ± 1.5	17.0 ± 1.3	17.0 ± 1.3	17.0 ± 1.3
Dex 20k (n=7)	1.76 ± 0.13	1.57 ± 0.12	1.52 ± 0.12	1.52 ± 0.12
Dex 70k (n=8)	1.47 ± 0.25	1.31 ± 0.22	1.25 ± 0.22	1.25 ± 0.22
IgG (n=7)	0.54 ± 0.10	0.48 ± 0.09	0.46 ± 0.09	0.46 ± 0.09
cAMP (Lp = 1 × 10^{-9} cm/s/cm H_2O)				
NaFl (n=9)	12.3 ± 1.2	11.0 ± 1.0	11.0 ± 1.0	11.0 ± 1.0
Dex 20k (n=7)	0.95 ± 0.13	0.85 ± 0.12	0.81 ± 0.12	0.81 ± 0.12
Dex 70k (n=8)	0.70 ± 0.09	0.62 ± 0.08	0.58 ± 0.08	0.58 ± 0.08
IgG (n=7)	0.31 ± 0.04	0.27 ± 0.04	0.26 ± 0.04	0.26 ± 0.04

Values are mean ± SE; n, number of vessels.